PCCP

Dynamic Article Links ►

Cite this: DOI: 10.1039/c0xx00000x

www.rsc.org/xxxxxx

PAPER

Time-resolved photoelectron imaging of the chloranil radical anion: Ultrafast relaxation of electronically excited electron acceptor states

Daniel A. Horke[a] and Jan R. R. Verlet*[a]

Received (in XXX, XXX) Xth XXXXXXXXX 20XX, Accepted Xth XXXXXXXXX 20XX

DOI: 10.1039/b000000x

The spectroscopy and dynamics of near-threshold excited states of the isolated chloranil radical anion are investigated using photoelectron imaging. The photoelectron images taken at 480 nm clearly indicate resonance-enhanced photodetachment via a bound electronic excited state. Time-resolved photoelectron imaging reveals that the excited state rapidly decays on a timescale of 130 fs *via* internal conversion. The ultrafast relaxation dynamics of excited states near threshold are pertinent to common electron acceptor molecules based on the quinone moiety and may serve as doorway states that enable efficient electron transfer in the highly exergonic inverted regime, despite the presence of large free energy barriers.

Introduction

Chloranil (CA) has been extensively used as an electron acceptor in artificial charge transfer complexes and salts.[1, 2] More generally, the chromophore of CA is a quinone, whose ubiquity as electron acceptors in nature is striking,[3] with examples ranging from photosynthesis[4, 5] and aerobic respiration[6, 7] to humic substances[8, 9] and natural sensors.[10, 11] Typically, quinone derivatives provide a large driving force for an electron transfer (ET) reaction and can often be characterised as being in the Marcus inverted region, where the rate of ET is reduced by a free energy barrier.[12] Despite this barrier, ET rates typically associated with near-barrierless reactions are commonly observed for quinones. Clear examples of this can be seen in the seminal work of Closs and Miller on the ET rates of donor-spacer-acceptor type molecules, in which the rate of ET is observed to be several orders of magnitude faster than predicted by Marcus theory.[13-16] While the participation of high-frequency vibrational modes is commonly invoked to explain such deviations in measured ET rates,[17] it is recognised that electronically excited states of the acceptor may also participate.[18-20] Here we consider electronically excited states of the radical anion of CA, which represent the product state of an ET reaction.

Quinone radical anions are reactive and generally short lived in solution and as a result, only a modest amount of information regarding their relaxation dynamics is known.[21, 22] Furthermore, experimental studies conducted in the condensed phase, either as a salt crystal or in solution, are expected to have their excited states strongly affected by the surroundings both in terms of energies and dynamics.[23] High level *ab initio* calculations naturally consider the isolated system and as a result, direct comparison of calculations with condensed phase data must be done with great care. In this article, we probe the ultrafast relaxation dynamics of the photo-excited chloranil radical anion ($CA^{\bullet-}$) in the gas-phase, using time-resolved photoelectron imaging.

CA is the fully chlorinated derivative of *p*-benzoquinone (*p*BQ) and serves as a representative quinone-based electron acceptor molecule. In fact, CA shares much of its excited state properties with *p*BQ, which has been more extensively studied than CA. CA is a planar molecule of D_{2h} symmetry and it owes much of its electron accepting ability to a large electron affinity (2.76 ± 0.2 eV).[24, 25] In solution, the absorption spectrum of $CA^{\bullet-}$ shows two broad features around 450 nm and 320 nm, with a shallow tail towards higher wavelengths.[26] This is broadly similar to the absorption spectrum of $pBQ^{\bullet-}$, for which the low energy tail has been attributed to two excited states of nπ* character, which are dipole forbidden. A similar explanation can be invoked to explain the $CA^{\bullet-}$ absorption spectrum, which is supported by calculations (see below and the ESI). The next two states in both $pBQ^{\bullet-}$ and $CA^{\bullet-}$, ^2A_u and $^2B_{3u}$, are bright. The ^2A_u corresponds to the excitation from the singly occupied $\pi^*(b_{2g})$ molecular orbital (corresponding to the lowest-unoccupied molecular orbital, LUMO, of neutral CA) to a higher-lying $\pi^*(a_u)$ molecular orbital. The $^2B_{3u}$ state is predominantly of $\pi^*(b_{2g}) \leftarrow \pi(b_{3u})$ character, in which an electron from a lower lying bonding orbital is promoted to the singly-occupied $\pi^*(b_{2g})$ and we term such a transition a core-transition. There is also a significant contribution from a $\pi^*(b_{3u}) \leftarrow \pi^*(b_{2g})$ transition. In $pBQ^{\bullet-}$, these states are very close in energy and both contribute to the absorption band at 450 nm, although their relative ordering has been debated and remains unclear.[23, 27] A similar debate has not been had for $CA^{\bullet-}$, but given the electronic similarity of $pBQ^{\bullet-}$ and $CA^{\bullet-}$, the absorption spectrum may be interpreted in a similar way. The relevant molecular orbitals are shown in Fig. 1(a) as well as an energy level diagram of $CA^{\bullet-}$ in Fig. 1(b), indicating the electronic states that are accessible in the current experiment.

Brauman and co-workers have measured the gas-phase absorption spectra for a number of radical anions,[28] highlighting that bound excited states of anions exist in certain systems. The gas-phase absorption spectrum of $CA^{\bullet-}$ is very similar to the

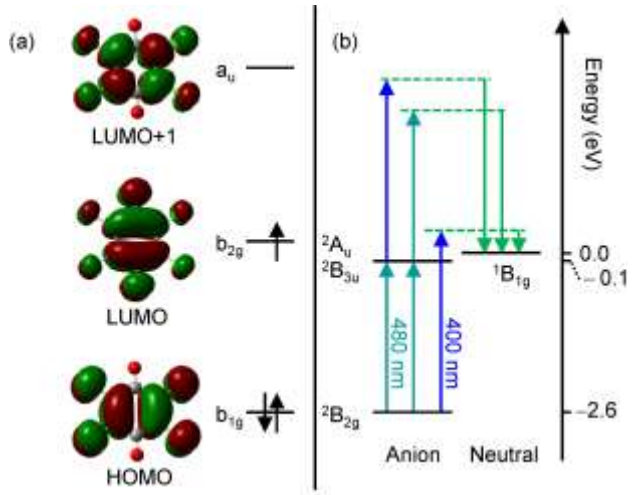

Fig. 1 (a) Relevant molecular orbitals and their occupancies for the chloranil radical anion. Excitation into the ^2A_u state corresponds to promotion of an electron from the LUMO to the LUMO+1. (b) Electronic state diagram for anionic and neutral chloranil, showing the pump-probe scheme employed for time-resolved studies.

solution phase spectrum and shows that there is strong absorbance below the electron affinity and these excited states will consequently be bound with respect to electron loss.

Electron attachment to gas-phase CA has shown that thermal electrons (~0 eV) predominantly form the long-lived $CA^{\bullet-}$ radical anion (with lifetimes > 1 μs),[24] suggesting that these threshold states can accept electrons. A minor channel, contributing less than 2%, corresponds to the loss of Cl^- following electron attachment. This channel exhibits a resonance at 0.9 eV above threshold, which was assigned to the ^2A_u state.[24] However, electron attachment experiments take place in the geometry of the neutral molecule. From calculations on *p*BQ,[23] the $^2B_{3u}$ is calculated to lie above ^2A_u in the neutral geometry, which suggests that it may be the ^2A_u state that accepts the electron that forms the long-lived $CA^{\bullet-}$.

Although the spectroscopy of $CA^{\bullet-}$ has been the focus of a number of studies,[26, 28, 29] there is no information regarding the excited state dynamics. From an ET perspective, the dynamics of the excited state in which the excess electron resides in the $\pi^*(a_u)$ orbital is of particular interest, as this does not involve any rearrangement of the core electrons. Furthermore, as the ^2A_u anionic state is nearly degenerate with the neutral ground state of CA, it can readily accept a low-energy electron. Other nearby excited anion states are of core-excited character and anion formation following the electron attachment into these states requires a concerted two-electron process. The likelihood of this is substantially lower, as is evident from the autodetachment spectra of the closely related $p\text{BQ}^{\bullet-}$.[30] The most dominant excitation observed (by a factor of ~50) in the autodetachment spectra of $p\text{BQ}^{\bullet-}$ is a broad shape resonance assigned to the $^2A_u \leftarrow {}^2B_{2g}$ transition. Narrow vibrational features of the $^2B_{3u}$ Feshbach resonance are also observed, suggesting that these are longer lived (ranging from 210 fs to >1.2 ps), with respect to autodetachment or internal conversion.[30] Here, we study the ultrafast relaxation dynamics following excitation to the ^2A_u or $^2B_{3u}$ states of $CA^{\bullet-}$ using time-resolved photoelectron imaging[31-33] and provide some evidence from the resonance-enhanced two-photon photodetachment spectra that the state that is predominantly excited is the ^2A_u.

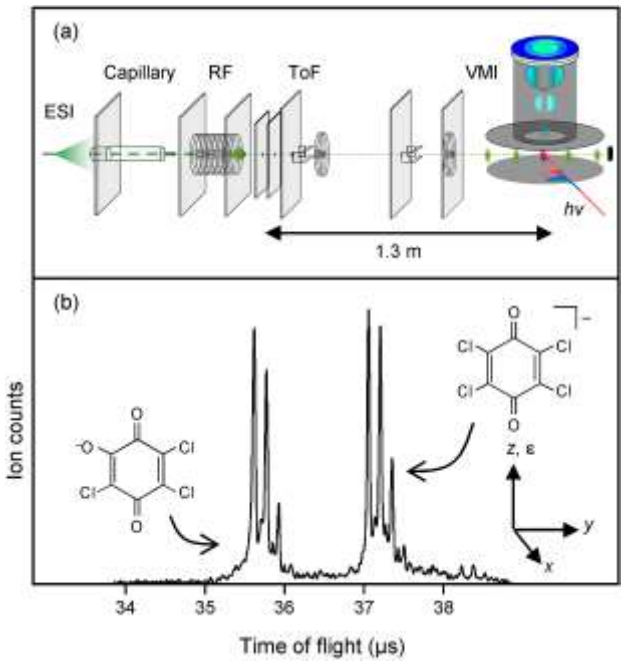

Fig. 2 (a) Schematic of the experimental setup, consisting of an electrospray ionisation source (ESI), a transfer capillary, a radio-frequency ion guide and trap (RF), a time-of-flight mass spectrometer (ToF) and a velocity-map imaging setup (VMI). (b) Time-of-flight spectrum obtained from ESI of a 1 mM solution of chloranil in acetonitrile. Clearly seen are the isotopic progressions for the radical anion of chloranil and deprotonated anion of the derivative in which one chlorine has been replaced by a hydroxide group

Experimental methods

The experimental apparatus has been described in detail elsewhere[34, 35] and only a brief overview with specific details pertaining to the current experiment is given. CA (99%, Sigma-Aldrich) is used without further purification to make a 1 mM solution of CA in acetonitrile. With reference to Fig. 2(a), the CA solution is transferred from a syringe pump to an electrospray ionisation source, held at around –2.4 kV, which produces a stable spray for several hours. The aerosol containing anions and solvent droplets is transferred to vacuum via a heated stainless steel capillary (80° C). After desolvation, ions are directed into a second vacuum chamber, where they are guided and trapped using a home-build radio-frequency ion guide. Ions are injected collinearly into a time-of-flight mass spectrometer and detected using a pair of multichannel plates (MCPs) following flight through a 1.3 m flight tube, containing focussing and steering optics. Fig. 2(b) shows a typical anion mass-spectrum. It contains two isotopic progressions which can be assigned to $CA^{\bullet-}$ and the deprotonated $C_6O_2Cl_3O^-$, which forms very easily in the presence of trace amounts of H_2O.[36]

The interaction time between ions and laser is chosen such that only the $CA^{\bullet-}$ is probed in the experiment. Femtosecond pulses are derived from a commercial chirped-pulse amplified Ti:Sapphire laser system producing 35 fs pulses with 2.7 W at 1 kHz. Approximately half of the 800 nm fundamental beam is used to pump an optical parametric amplifier (TOPAS),

producing 1200 nm in the signal, which is subsequently mixed with 800 nm fundamental light in a type-II beta-barium borate (BBO) crystal to produce 480 nm pulses with energies of ~100 μJ pulse^{-1}. About half of the remainder of the fundamental beam is used for second harmonic generation in a type-I BBO crystal, producing ~100 μJ pulse^{-1} at 400 nm. Pulses are delayed relative to each other using a motorised optical delay line. Both laser beams are collinearly combined and intersect the ion beam perpendicularly at the centre of a velocity-map imaging (VMI) arrangement, which collects electrons in the direction mutually perpendicular to the ion and laser beams. The VMI setup uses an electrostatic emersion lens to focus the velocities of electrons originating from different points in the interaction volume onto the same point at a focal plane determined by the VMI setup.[37] In the current arrangement, a resistive glass tube is employed to form a constant electric field gradient, which allows the VMI to be operated at very low voltages (–250 V) and does not affect the ion beam propagation.[34] At the focal plane a pair of MCPs coupled to a phosphor screen allows a CCD camera to monitor the position of electrons on the 2D plane. This 2D "raw image" is subsequently deconvoluted by removing the azimuthal contribution using the poplar-onion peeling (POP) routine.[38] The angularly integrated radial spectra are proportional to the velocity and are then converted into photoelectron (PE) spectra. In addition to the PE spectra, the PE angular distributions (PADs) are also recorded and can provide additional information about the orbitals from which electrons are removed. PADs can also be used to gain further information concerning the relaxation dynamics.[34] PE images are collected for approximately 2×10^5 laser shots and the PE spectra have been calibrated using the PE spectrum of I^- at 4.66 eV (266 nm), providing a resolution of $\Delta E/E = 5\%$.

The polarisation, **ε**, of both laser beams is parallel to the plane of the detector. The laser beam at the interaction point is ~2 mm in diameter, corresponding to a laser pulse intensity of ~3×10^{10} W cm^{-2}, which is below typical intensities required to drive non-linear (multi-photon) processes. The cross correlation between the 480 nm and 400 nm beams has been measured outside the vacuum chamber using a thin BBO crystal and was found to be on the order of 130 fs. This measurement has been calibrated with a cross correlation measured inside the vacuum chamber using above-threshold detachment of I^-.

Results and discussion

Photoelectron spectroscopy of the Chloranil anion

The PE spectra of $CA^{\bullet-}$ have been measured at 3.10 eV (400 nm) and 2.58 eV (480 nm) and are shown in Fig. 3(a) and (b) respectively. The insets show the respective central slice through the reconstructed PE cloud. At 3.10 eV, a broad unresolved low-energy feature is observed with an electron kinetic energy (*eKE*) extending to ~0.6 eV. From this, the adiabatic detachment energy is estimated to be 2.60 ± 0.1 eV, which is in reasonable agreement with measurements that have determined the electron affinity to be 2.76 ± 0.2 eV.[24, 25]

At 2.58 eV, the photon energy is expected to be predominantly below the detachment energy. This is in line with the observed PE spectrum (Fig. 3(b)), where firstly, the signal levels are

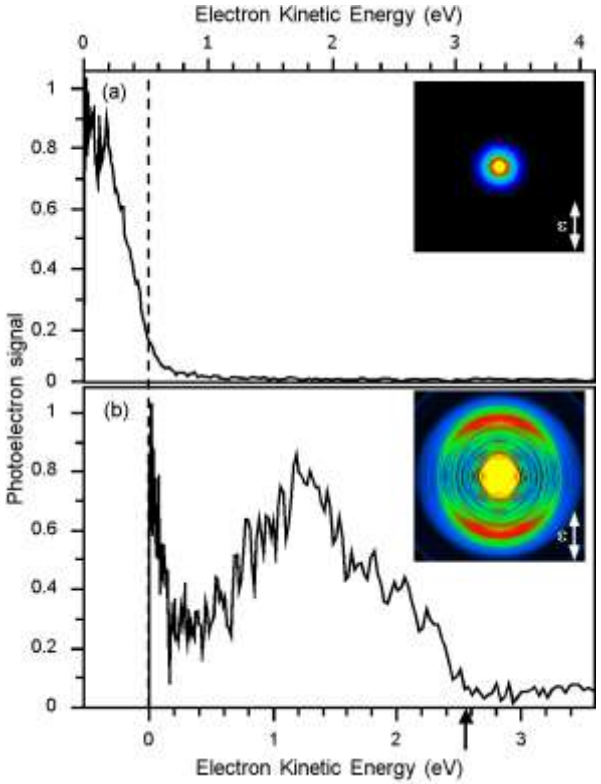

Fig. 3 Photoelectron spectra of the chloranil radical anion. (a) Spectrum collected at 3.10 eV photon energy, showing a strong feature from direct detachment, extending to ~0.6 eV kinetic energy. (b) Spectrum collected at 2.58 eV photon energy, showing a weak low *eKE* feature from direct detachment and a strong feature around 1.2 eV from two-photon resonant enhanced detachment. The energy scales in (a) and (b) are offset by the difference in photon energy used (0.52 eV); this is indicated by the vertical dashed line. Shown inset are the deconvoluted photoelectron images.

significantly lower than for the 400 nm spectrum (by a factor of ~12 with respect to Fig. 3(a)) and secondly the feature at low *eKE* has almost completely disappeared. The small peak below 0.2 eV is due to a small amount of direct detachment presumably enabled by the broad Franck-Condon window. The spectra shown in Fig. 3 are offset with respect to each other by the difference in photon energy used (0.52 eV), as indicated by the vertical dashed line. Comparing the spectrum recorded at 3.10 eV (400 nm) in Fig. 3(a) with that taken at 2.58 eV (480 nm) in (b) indicates that indeed a small amount of direct 1-photon detachment is expected at 2.58 eV. The most prominent feature in the 2.58 eV PE spectrum, however, is the broad anisotropic feature centred around 1.2 eV, with observed anisotropy parameters $\beta_2 = 0.6 \pm 0.3$ and $\beta_4 = -0.1 \pm 0.2$. This arises from the resonance-enhanced 2-photon detachment (R2PD) via the ^2A_u or $^2B_{3u}$ states, which have a maximum around 2.75 eV (450 nm) in solution. The assignment to a resonance-enhanced process is supported by the lack of a R2PD feature in the 3.10 eV PE spectrum, which is not resonant with any major features in the absorption spectrum. The two 2.58 eV photons impart a combined energy of 5.16 eV to the system, such that this feature is expected to extend to *eKE* = 2.56 eV, if the final state corresponds to the neutral $^1B_{1g}$ ground state. This is consistent with the observed PE spectrum, as indicated in Fig. 3(b) by the vertical arrow. While both the ^2A_u and $^2B_{3u}$ states are energetically accessible and could partake in the dynamics,

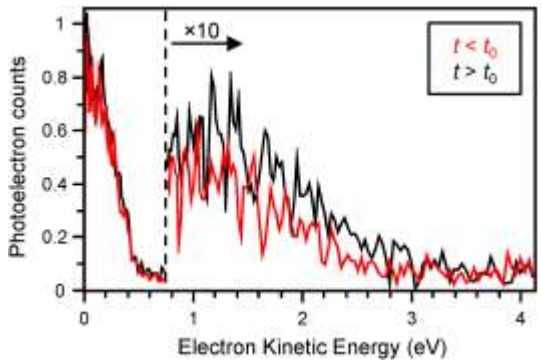

Fig. 4 Representative photoelectron spectra before t_0 (red trace, probe before pump) and after t_0 (black trace, pump before probe). At positive times the observed two-photon detachment feature shifts to higher kinetic energies due to the higher photon energy of the pump photon.

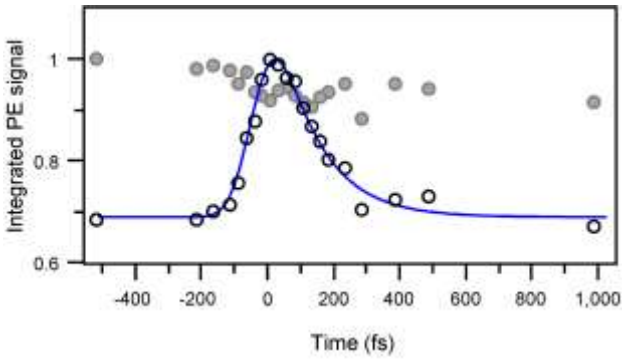

Fig. 5 Integrated photoelectron signals as a function of pump-probe delay. Open circles correspond to the integrated PE signal due to the pump and probe pulses (1.0 < *eKE* < 3.1 eV) and reflects the excited state population; solid grey circles reflect the ground state population (0.0 < *eKE* < 0.4 eV). The solid line is a fit to the excited state dynamics and yields a lifetime of 130 fs.

only the ^2A_u state fully correlates with the neutral ground state. Specifically, removal of the single electron from the $\pi^*(a_u)$ orbital generates CA in its $^1B_{1g}$ neutral ground state. In contrast, the $^2B_{3u}$ state is predominantly of core-excited character. Removal of an electron from the doubly occupied $\pi^*(b_{2g})$ orbital would leave the remaining neutral in an excited triplet state and would either show up in the recorded PE spectrum at low *eKE*, if the triplet state is accessible, or not at all if the relevant triplet state of the neutral is inaccessible. There is no evidence of triplet CA formation, suggesting that we predominantly excited the ^2A_u state, although we note that the $^2B_{3u}$ state is expected to be of mixed character and minor contributions can correlate with the ground state of CA.

The width of the R2PD spectrum suggests that either the excited state undergoes significant rearrangement following excitation, or that there is a large geometric change to the neutral ground state. As the R2PD spectrum was collected using ~100 fs pulses, the former effect is likely to be limited as there is insufficient time for a major geometric change over the duration of the pulse. Instead, the more likely factor leading to the spectral width is the change in geometry between the anion ground and neutral ground state (the anion excited state is formed in the anion ground state geometry). We have performed time-dependent density functional calculations (TD-DFT) with the B3LYP functional and cc-pVTZ basis set using the Gaussian09 package[39] to gain a qualitative understanding of the relevant orbitals and electronic excited states of CA. The CA molecule has D_{2h} symmetry in both neutral and anion ground states. In Fig. 1, the HOMO (b_{1g}), LUMO (b_{2g}) and LUMO+1 (a_u) of CA are shown. The $\pi^*(a_u) \leftarrow \pi^*(b_{2g})$ transition corresponds to excitation of the anion from the singly-occupied LUMO to the LUMO+1, which is a ^2A_u state. From the MO picture, the origin of the PE spectral width is apparent. In going from the anion ground state to the neutral ground state (HOMO ← LUMO), the π^* character along the C=O bonds of the anion is removed and this bond therefore is expected to shorten significantly upon detachment. This has also been noted in other theoretical studies[40, 41] and is the main contribution to the observed broadening in the PE spectrum. There is some evidence of a vibrational progression at high *eKE* in the R2PD feature in Fig. 3. However, given our initial ion temperature of ~ 300K, that we are performing the R2PD using broadband pulses, and that the intrinsic resolution is 0.1 eV at *eKE* = 2 eV; performing a detailed analysis on these features is not sufficiently accurate to provide additional insight.

Time-resolved photoelectron spectroscopy

In order to study the dynamics of the excited state, we use a two colour pump-probe scheme, shown in Fig. 1(b). A femtosecond pulse at 2.58 eV (480 nm, pump) is used to transfer population to the excited state, which is subsequently probed at various delays using a pulse at 3.10 eV (400 nm, probe). The probe photon energy has been chosen such that it is sufficient to monitor both excited and ground state populations, and, in principle, any intermediate excited states that may be populated. Excitation at 2.58 eV produces the PE spectrum in Fig. 3(b). If the excited state is probed at 3.10 eV, then the additional energy imparted to the system will result in a shift of the observed R2PD PE spectrum to higher *eKE* by 0.52 eV, extending the spectrum out to ~3.1 eV. Two representative PE spectra, one at negative time (probe before pump) and one near zero delay (pump and probe are overlapping) are presented in Fig. 4. These show that the PE spectrum does indeed extend to higher energy at t = 0. The difference between the two spectra clearly shows the excited state signal.

The relaxation dynamics of the excited state are monitored by integrating the PE spectra over an *eKE* window, representative of the excited state. In Fig. 5, the total PE signal from 1.0 to 3.1 eV is shown. This clearly shows an increase in PE signal, which arises from the overlapping pump and probe pulses, followed by a very rapid decay of the excited state population. In order to extract the excited state lifetime, we fit the PE intensity, I_{PE}, to a single exponential decay convoluted with a Gaussian instrument response function:[42]

$$I_{PE} = I_0 + A_0 \exp\left(-\frac{t-t_0}{\tau}\right) erfc\left(\frac{\sigma_L}{\sqrt{2}\tau} - \frac{t-t_0}{\sqrt{2}\sigma_L}\right), \qquad (1)$$

where A_0 is an amplitude factor, τ is the excited state lifetime, σ_L is related to the full-width at half maximum of the laser cross-correlation ($\mathrm{FWHM} = \sigma_L\sqrt{8\ln 2}$), *erfc* is the complementary error function and I_0 is an offset to account for background PE signal. The fit to the convoluted data is shown as a solid line in Fig. 5 and yields an excited state lifetime of τ = 130 ± 30 fs. This is very close to the time-resolution of the experiment as

determined by the cross-correlation (130 fs). Hence, although the fit in Fig. 5 clearly does reproduce the exponential decay, the measured lifetime should be taken as an upper-limit.

The observed dynamics are associated with a loss of population from the excited state. Internal conversion occurring on ~100 fs timescales is usually associated with a conical intersection. The excited state is initially formed in the geometry of the anion $^2B_{2g}$ ground state and will subsequently evolve to a geometry at which there is a conical intersection with some other excited state of the system. Conical intersections often involve out-of-plane deformations and these are the modes predicted to be predominantly excited following $^2A_u \leftarrow {}^2B_{2g}$ excitation,[23] providing additional evidence that the dynamics reflect the population in the ^2A_u state.

The vibrational dynamics on an excited state can be discerned in time-resolved PE spectroscopy as temporal changes in the *eKE*. Although the data is not of sufficient quality to observe such changes by inspection, a weighted mean of the background subtracted PE spectra (in which a $t < 0$ PE spectrum has been subtracted from all time-resolved PE spectra leaving only the pump-probe feature) provides a representative measure of the average *eKE* as a function of time. This shows no appreciable change over the course of the relaxation, but given the width of the PE spectrum, this is perhaps not surprising. Furthermore, dynamics in the *eKE* will only be evident as long as the excited (^2A_u) and final ($^1B_{1g}$) states' energy difference changes along the vibrational coordinate of interest. This is not necessarily the case here. Nevertheless, the lack of spectral change in *eKE* does suggest that the ^2A_u state population is not lost to excited state autodetachment. This could occur if the geometric changes in the ^2A_u state move it above the neutral $^1B_{1g}$ state energy. Indeed, PE produced with very high energy ($2.9 < eKE < 3.1$ eV) are susceptible to direct autodetachment based on the one-colour PE spectrum shown in Fig. 3(b). Unfortunately, signal levels are very low in this window and actually present a very minor contribution to the dynamics in Fig. 5. Furthermore, vibrational excited state autodetachement would be accompanied by very low *eKE*,[43] but no discernable dynamics are observed at low *eKE*, as is discussed below.

A useful feature of anion time-resolved PE spectroscopy is that, in general, ground state recovery dynamics can also be observed. In the current experiment, this should be the case because the 3.1 eV probe has sufficient energy to remove an electron from the $^2B_{2g}$ ground state of the anion. In Fig. 5, we also show the normalised integrated PE signal from $0 < eKE < 0.4$ eV, which should capture most of the dynamics arising from the ground state. However, it is evident that there are no clear temporal changes in this, with the exception of a marginal depletion at $t = 0$. The population transferred to the excited state is small because of the small excitation cross section. Observing such small changes on the large background is within the noise of our experiment and we do not observe the concomitant ground state recovery. Moreover, this spectral window is convoluted with PE originating from other potential processes. Specifically, our calculations suggest that there are two lower-lying excited states in the vicinity of the ^2A_u state that are of nπ^* character (see ESI). In pBQ$^{\bullet-}$, these states contribute to the low-energy tail observed in the absorption spectrum. Population could in principle cascade down via internal conversion to these nπ^* states. Such dynamics are typically reflected in PE spectra as red-shifts in *eKE*.[44, 45] In the current system however, the nπ^* states require an additional electronic rearrangement upon photo-detachment to correlate to the $^1B_{1g}$ ground state of the neutral. This process is likely to have a very low cross section and the more likely detachment channel is to produce neutral CA in its triplet excited state.[29] This will produce low energy PEs in the $0 < eKE < 0.4$ eV range shown in Fig. 5. As mentioned, there are insufficient changes in the PE signal to observe such dynamics or ground-state recovery dynamics. Hence, although we can conclude the excited state is short-lived and that the dynamics involve internal conversion, we cannot definitively assign the states to which population is transferred. Note also that the additional 0.52 eV imparted by the probe should make the triplet state of the neutral, to which the $^2B_{3u}$ excited state correlates, accessible if it was excited. This would be evidenced by an increase at low *eKE*. Our observation of a decrease due to ground state depletion contradicts this and provides further evidence that the state predominantly excited is the ^2A_u state.

From an isolated electron acceptor perspective the instantaneous addition of an electron to CA in the near-threshold ^2A_u excited state rapidly leads to an exchange of electronic to vibrational energy in CA$^{\bullet-}$. In a condensed phase environment, the excess vibrational energy, which is rapidly redistributed, can then be lost to the surroundings, stabilising the CA$^{\bullet-}$ radical anion. As a result, the ^2A_u excited state would act as an efficient doorway state facilitating electron capture in the highly exergonic inverted region of ET reactions. The observation of long-lived CA$^{\bullet-}$ following capture by CA of slow electrons[24] complements the observation that the energy can be rapidly redistributed into vibrational modes.

The ultrafast relaxation dynamics of the near threshold excited state in the related tetrafluoro-tetracyanoquinodimethane radical anion (F_4-TCNQ$^{\bullet-}$) have also recently been studied in our group.[46] In this, very rapid sub-100 fs relaxation timescales have been observed and interpreted as a fast internal conversion process *via* a conical intersection with the ground anionic state. Both F_4-TCNQ$^{\bullet-}$ and CA$^{\bullet-}$ are part of the quinone family and we speculate that it may be the dynamics of the quinone moiety that are ultimately responsible for the observed relaxation dynamics. This argument is similar in spirit to many theoretical studies on conical intersections, which consider chromophores to represent the dynamics of much larger systems. Many ET reactions to quinone-derived electron acceptors lead to enhanced ET rates, which may be a direct result of the transfer to electronically excited states that efficiently couple to the ground state. We hope that our results will inspire theoretical studies to elucidate the relaxation dynamics and to determine if the dynamics are indeed a general feature of the quinone moiety.

Conclusions

Photoelectron imaging of the radical anion of chloranil (CA$^{\bullet-}$) has been presented. Excitation above threshold (3.10 eV, 400 nm) yields a feature arising from the direct detachment and provides an adiabatic detachment energy of 2.60 ± 0.1 eV. Excitation at 2.58 eV (480 nm) is resonant with the ^2A_u and $^2B_{3u}$ excited states in CA$^{\bullet-}$. The clear two-photon resonance-enhanced photoelectron

feature is predominantly due to excitation to the ^2A_u state. Time-resolved photoelectron imaging has been used to study the relaxation dynamics of near-threshold excited states in $CA^{\bullet-}$. The dynamics reveal that excited state population decays within 130 ± 30 fs *via* internal conversion, either to lower lying excited states of nπ* character, or directly to the ground $^2B_{2g}$ state $CA^{\bullet-}$.

The observation of excited states near threshold in quinone-derivatives is pertinent to electron transfer (ET) reactivity in which quinones are common acceptors, both in artificial and natural charge-transfer complexes. The ^2A_u excited state in $CA^{\bullet-}$, which is the acceptor product of an ET reaction, can play an active role in accepting an electron and efficiently channel this towards the ground state of $CA^{\bullet-}$ by transferring electronic energy into vibrational energy on a 100 fs timescale. Excited states of quinones in general could act as efficient doorway states to electron transfer and can be used to explain the anomalously high rate constants observed for ET reactions in the inverted region.

Acknowledgements

This work has been supported by the EPSRC (EP/D073472/1) and the University of Durham.

Notes and references

[a] *Department of Chemistry, University of Durham, South Road, Durham DH1 3LE, United Kingdom. Tel: +44191 3342159; E-mail: j.r.r.verlet@durham.ac.uk*

Electronic Supplementary Information (ESI) available: Details of electronic structure calculations. See DOI:

1. W. L. Peticolas, *J. Chem. Phys.*, 1957, **26**, 429-430.
2. J. J. Mayerle, J. B. Torrance and J. I. Crowley, *Acta Cryst. B*, 1979, **35**, 2988-2995.
3. J. P. Klinman and D. Mu, *Annu. Rev. Biochem.*, 1994, **63**, 299-344.
4. P. R. Chitnis, *Annu. Rev. Plant. Physiol. Plant. Mol. Biol.*, 2001, **52**, 593-626.
5. G. Renger and T. Renger, *Photosynth. Res.*, 2008, **98**, 53-80.
6. T. M. Iverson, C. Luna-Chavez, G. Cecchini and D. C. Rees, *Science*, 1999, **284**, 1961-1966.
7. V. Yankovskaya, R. Horsefield, S. Törnroth, C. Luna-Chavez, H. Miyoshi, C. Léger, B. Byrne, G. Cecchini and S. Iwata, *Science*, 2003, **299**, 700-704.
8. R. M. Cory and D. M. McKnight, *Environ. Sci. Technol.*, 2005, **39**, 8142-8149.
9. D. T. Scott, D. M. McKnight, E. L. Blunt-Harris, S. E. Kolesar and D. R. Lovley, *Environ. Sci. Technol.*, 1998, **32**, 2984-2989.
10. J. J. Hickman, D. Ofer, P. E. Laibinis, G. M. Whitesides and M. S. Wrighton, *Science*, 1991, **252**, 688-691.
11. I. Willner and A. Riklin, *Anal. Chem.*, 1994, **66**, 1535-1539.
12. R. A. Marcus and N. Sutin, *Biochim. Biophys. Acta*, 1985, **811**, 265-322.
13. G. L. Closs, L. T. Calcaterra, N. J. Green, K. W. Penfield and J. R. Miller, *J. Phys. Chem.*, 1986, **90**, 3673-3683.
14. G. L. Closs and J. R. Miller, *Science*, 1988, **240**, 440-447.
15. J. R. Miller, J. V. Beitz and R. K. Huddleston, *J. Am. Chem. Soc.*, 1984, **106**, 5057-5068.
16. J. R. Miller, L. T. Calcaterra and G. L. Closs, *J. Am. Chem. Soc.*, 1984, **106**, 3047-3049.
17. P. F. Barbara, T. J. Meyer and M. A. Ratner, *J. Phys. Chem.*, 1996, **100**, 13148-13168.
18. A. Morandeira, L. Engeli and E. Vauthey, *J. Phys. Chem. A*, 2002, **106**, 4833-4837.
19. J. Petersson, M. Eklund, J. Davidsson and L. Hammarström, *J. Phys. Chem. B*, 2010, **114**, 14329-14338.
20. D. Rehm and A. Weller, *Isr. J. Chem.*, 1970, **8**, 259.
21. H. Görner and C. von Sonntag, *J. Phys. Chem. A*, 2008, **112**, 10257-10263.
22. A. R. Cook, L. A. Curtiss and J. R. Miller, *J. Am. Chem. Soc.*, 1997, **119**, 5729-5734.
23. Y. Honda, M. Hada, M. Ehara and H. Nakatsuji, *J. Phys. Chem. A*, 2002, **106**, 3838-3849.
24. C. D. Cooper, W. F. Frey and R. N. Compton, *J. Chem. Phys.*, 1978, **69**, 2367-2374.
25. P. Kebarle and S. Chowdhury, *Chem. Rev.*, 1987, **87**, 513-534.
26. J. J. Andre and G. Weill, *Mol. Phys.*, 1968, **15**, 97 - 99.
27. R. Pou-Amérigo, L. Serrano-Andrés, M. Merchán, E. Ortí and N. Forsberg, *J. Am. Chem. Soc.*, 2000, **122**, 6067-6077.
28. E. A. Brinkman, E. Gunther, O. Schafer and J. I. Brauman, *J. Chem. Phys.*, 1994, **100**, 1840-1848.
29. D. R. Kemp and G. Porter, *J. Chem. Soc. D*, 1969, 1029-1030.
30. J. Schiedt and R. Weinkauf, *J. Chem. Phys.*, 1999, **110**, 304-314.
31. R. Mabbs, E. R. Grumbling, K. Pichugin and A. Sanov, *Chem. Soc. Rev.*, 2009, **38**, 2169-2177.
32. A. Stolow, A. E. Bragg and D. M. Neumark, *Chem. Rev.*, 2004, **104**, 1719-1758.
33. J. R. R. Verlet, *Chem. Soc. Rev.*, 2008, **37**, 505-517.
34. J. Lecointre, G. M. Roberts, D. A. Horke and J. R. R. Verlet, *J. Phys. Chem. A*, 2010, **114**, 11216-11224.
35. G. M. Roberts, J. Lecointre, D. A. Horke and J. R. R. Verlet, *Phys. Chem. Chem. Phys.*, 2010, **12**, 6226-6232.
36. D. H. Sarr, C. Kazunga, M. J. Charles, J. G. Pavlovich and M. D. Aitken, *Environ. Sci. Technol.*, 1995, **29**, 2735-2740.
37. A. T. J. B. Eppink and D. H. Parker, *Rev. Sci. Instrum.*, 1997, **68**, 3477-3484.
38. G. M. Roberts, J. L. Nixon, J. Lecointre, E. Wrede and J. R. R. Verlet, *Rev. Sci. Instrum.*, 2009, **80**, 053104.
39. Gaussian 09, Revision A.1, M. J. Frisch, G. W. Trucks, H. B. Schlegel, G. E. Scuseria, M. A. Robb, J. R. Cheeseman, G. Scalmani, V. Barone, B. Mennucci, G. A. Petersson, H. Nakatsuji, M. Caricato, X. Li, H. P. Hratchian, A. F. Izmaylov, J. Bloino, G. Zheng, J. L. Sonnenberg, M. Hada, M. Ehara, K. Toyota, R. Fukuda, J. Hasegawa, M. Ishida, T. Nakajima, Y. Honda, O. Kitao, H. Nakai, T. Vreven, J. A. Montgomery, Jr., J. E. Peralta, F. Ogliaro, M. Bearpark, J. J. Heyd, E. Brothers, K. N. Kudin, V. N. Staroverov, R. Kobayashi, J. Normand, K. Raghavachari, A. Rendell, J. C. Burant, S. S. Iyengar, J. Tomasi, M. Cossi, N. Rega, J. M. Millam, M. Klene, J. E. Knox, J. B. Cross, V. Bakken, C. Adamo, J. Jaramillo, R. Gomperts, R. E. Stratmann, O. Yazyev, A. J. Austin, R. Cammi, C. Pomelli, J. W. Ochterski, R. L. Martin, K. Morokuma, V. G. Zakrzewski, G. A. Voth, P. Salvador, J. J. Dannenberg, S. Dapprich, A. D. Daniels, Ö. Farkas, J. B. Foresman, J. V. Ortiz, J. Cioslowski, and D. J. Fox, Gaussian, Inc., Wallingford CT, 2009.
40. S. E. Boesch and R. A. Wheeler, *J. Phys. Chem. A*, 1997, **101**, 8351-8359.
41. C. Katan, P. E. Blöchl, P. Margl and C. Koenig, *Phys. Rev. B*, 1996, **53**, 12112.
42. D. Hanggi and P. W. Carr, *Anal. Chem.*, 1985, **57**, 2394-2395.
43. B. Baguenard, J. C. Pinaré, C. Bordas and M. Broyer, *Phys. Rev. A*, 2001, **63**, 023204.
44. A. E. Bragg, J. R. R. Verlet, A. Kammrath, O. Cheshnovsky and D. M. Neumark, *J. Chem. Phys.*, 2005, **122**, 054314.
45. J. R. R. Verlet, A. E. Bragg, A. Kammrath, O. Cheshnovsky and D. M. Neumark, *J. Chem. Phys.*, 2004, **121**, 10015-10025.
46. D. A. Horke, G. M. Roberts and J. R. R. Verlet, *J. Phys. Chem. A*, 2011, **115**, 8369-8374.